JOURNAL OF MULTIFUNCTIONAL MATERIALS & PHOTOSCIENCE
12(1), June 2021, pp. 1-24

New Tailoring of Photocatalysts for the Reduction of CO_2 : Photocatalytic and Electrochemical Reaction

Zambaga Otgonbayar[1], Chang Sung Lim[1], Suresh Sagadevan[2], Kyung-Sang Cho[3], Saksit Chanthai[4], Won-Chun Oh[1*]

[1] Department of Advanced Materials Science & Engineering, Hanseo University, Chungnam 356-706, South Korea*
[2]Nanotechnology & Catalysis Research Centre, University of Malaya, Kuala Lumpur, Malaysia
[3]Department of Biocosmetics, Incheon Jaeneung University, Incheon 22573, South Korea
[4]Materials Chemistry Research Center, Department of Chemistry and Center of Excellence for Innovation in Chemistry, Faculty of Science, Khon Kaen University, Khon Kaen 40002, Thailand

Abstract: The electrochemical carbon dioxide reduction reaction (CO_2RR) provides an attractive approach to convert renewable electricity into fuels and feedstocks in the form of chemical bonds. Specially, the manufacture of methanol is more advantageous than methane and carbon monoxide. The designing of the novel-structured catalyst is the main feature how the carbon dioxide converts into hydrocarbon fuels. The most importantly, effective charge transfer property between 2D-structure graphene and semiconductor is the main feature of the photocatalyst. Nowadays, the ternary nanocomposite had better activity than binary and unary nanocomposite, and each semiconductor in the ternary nanocomposite has specific physical and chemical properties. This review paper mainly presents the influence of various factors on the photocatalytic performance, the type of photocatalyst and the reaction mechanism.

Keywords: CO_2 reduction, electrochemical, photocatalytic, semiconductor, 2D graphene, metal nanocomposite, ternary nanocomposite.

1. Introduction

The increasing greenhouse gas CO_2 concentration level in atmosphere raises serious concerns on fossil fuel-based energy supply. Renewable energy sources, such as solar, wind, hydro, and waves, are being considered as potential alternatives because they are more sustainable and carbon-neutral. Carbon dioxide (CO_2) is a kinetically and thermodynamically stable molecule, thus CO_2 conversion reactions are endothermic and need efficient catalysts to obtain high yield. Since late 19th century, CO_2 concentration in the atmosphere has increased from 280 to 400 ppm [1, 2]. This has resulted in the continuous rise of the global average temperature. How to effectively reduce the atmospheric CO_2 level and further utilize it has become an important research topic

* Corresponding author: *E-mail: wc_oh@hanseo.ac.kr*

worldwide. Strategies are now being actively sought to mitigate CO_2 emission via improving the combustion efficiency of fossil fuels or exploring clean and renewable energy sources (e.g., wind, tide, and solar energy) [3, 4, 5]. Alternatively, great efforts are also being actively undertaken to develop carbon capture and storage (CCS) techniques that fix atmospheric CO_2 and store it underground in a supercritical state. Fossil fuel is one of the largest energy sources in the world and their continuously combustion is belonging to the primary producer of carbon dioxide in the atmosphere. For the past few decades, there has been an increased interest in the carbon mitigation plan. CO_2 is one of the most stable molecules due to the strong C-O double bond with bonding energy of 750 kJ x mol^{-1} considerably larger than that of C-C (336 kJ x mol^{-1}), C-O (327 kJ x mol^{-1}), or C-H bond (411 kJ x mol^{-1}). CO_2 reduction via either the electrocatalytic or the photocatalytic approach is a thermodynamically uphill reaction and demands significant energy input to break the C-O bond. To make it even more complicated, CO_2 reduction may proceed via several different reaction pathways with the transfer of 2, 4, 6, 8, 12 or even more electrons and yielding diverse reduction products including carbon monoxide (CO), formic acid (HCOOH), methane (CH_4), ethylene (C_2H_4), and many others depending on the nature of the electrocatalysts or photocatalysts as well as the actual experimental conditions [6, 7]. As a result, electrocatalytic or photocatalytic CO_2 reduction is generally suffered from very limited efficiency and poor selectivity.

1.1. Electrochemical CO_2 reduction

The electrochemical reduction of carbon dioxide is the conversion of carbon dioxide to more reduced chemical species using electrical energy. It is one possible step in the broad scheme of carbon capture and utilization. The first examples of electrochemical reduction of carbon dioxide are from the 19th century, when carbon dioxide was reduced to carbon monoxide using a zinc cathode. Research in this field intensified in the 1980s following the oil embargoes of the 1970s. Electrochemical reduction of carbon dioxide represents a possible means of producing chemicals or fuels [8-11]. There are several important performance metrics in the evaluation of CO_2 reduction electrocatalysts as listed in the following: onset potential (onset potential refers to the working potential where the electrocatalytic current starts to take off from the background), Tafel slope (corresponds to a steep rise of the current density with the increasing overpotential and is a highly desirable characteristic of electrocatalysts) [12], turnover frequency (defined as the rate of electrochemical conversions per electrocatalytic site at certain overpotential) [13], faradaic efficiency (certain product is defined as the ratio of charges transferred to this product relative to the total charges passed through the circuit), stability (critical step toward the continuous optimization of electrocatalysts).

1.2. Photocatalytic CO_2 reduction

The photocatalytic CO_2 reduction process mainly conducted by using a semiconductor photocatalyst. [14]. It consists of five sequential steps—light absorption, charge separation,

CO_2 adsorption, surface redox reaction, and product desorption. The first step is the absorption of photons to generate electron and hole pairs. An illumination of a photocatalyst with the incident light excites electrons from the valance band (VB) to the conduction band (CB), leaving an equal number of holes in VB. In order for these photogenerated electrons or holes to be energetically favorable to reduce CO_2 or oxidize water, photocatalysts should possess a suitable band structure. Their CB edge must be more negative than the redox potential of CO_2 reduction, and the VB edge should be more positive than the redox potential of water oxidation (0.817 V vs SHE in pH 7.0 aqueous solution) [15]. The bandgap has to be sufficiently large since we need to additionally take into consideration the large overpotentials associated with these two electrochemical reactions. On the other hand, the band gap of photocatalysts cannot be too large as this would limit their effective utilization of the solar spectrum. The second step is the spatial separation of photogenerated electrons and holes. This process is in direct competition with the charge recombination. Whether the charge separation is dominant over the recombination or vice versa depends on the relative time scale between the lifetime of photogenerated carriers and the recombination rate and is determined by a complex interplay among material crystallinity, dimension, surface properties, and many other structural factors. Pronounced recombination would result in the significant loss of free charge carriers and the release of harvested energy as heat. To enhance the overall photocatalytic efficiency therefore requires improving the separation efficiency of photogenerated carriers and suppressing their possible recombination. It may be achieved via the proper modification of material structures, such as selective surface treatments. The third step is the CO_2 adsorption. It is the prerequisite for the electron transfer from the photocatalyst to the CO_2 molecule. In general, photocatalysts with high surface areas can provide more active sites for the CO_2 adsorption [16, 17]. Another possible route to improve the CO_2 adsorption is the alkali modification of the photocatalyst surface. The fourth step is the surface redox reaction. After migrating to the surface, photogenerated electrons and holes can separately drive different half reactions: electrons for reducing CO_2 to CO, CH_4, HCOOH, CH_3OH or other hydrocarbons, and holes for oxidizing water to molecular O_2. This step is a purely electrochemical process. The introduction of cocatalysts for CO_2 reduction or water oxidation would dramatically enhance the interfacial charge transfer rate, and hence the overall solar to fuel conversion efficiency (SFE). Optimal electrocatalysts identified from electrochemical studies are also good candidates as cocatalysts, given that a suitable interface is established between the semiconductor photocatalyst and cocatalyst to enable the rapid charge transfer across it. This step also clearly reflects the interesting connection between electrocatalysis and photocatalysis. After the photocatalytic reaction is complete, the last step is product desorption.

In addition, photocatalysis has the following two important performance metrics that are frequently cited in literature: *Apparent quantum efficiency (AQE) or external quantum efficiency (EQE)*: AQE or EQE is defined as the number ratio of electrons transferred toward a certain product relative to incident photons at a given wavelength [18]. They can be expressed as the product of the efficiencies of light absorption, charge separation,

and surface redox reaction. SFE is defined as the ratio of converted chemical energy relative to the incident solar energy. It can also be understood as the integral of AQE or EQE over the entire solar spectrum [19].

In the last few decades, intensive investigations have been conducted to improve the efficiency of photocatalytic CO_2 reduction using water (H_2O) as the hole scavenger, ranging from the exploration of novel catalysts [20], [21], bandgap engineering [22], recombination inhibition [23], to system optimization [24], [25]. Photocatalytic reduction includes photo-generated charge carrier behaviors inside photocatalysts and surface reactions, so both of them should be considered in evaluating the STF efficiency. Especially for the photocatalytic CO_2 reduction in water, the gas adsorption is of the first concern during the complicated gas-liquid-solid reaction because the reaction kinetics is highly correlated with the surface gas concentration [26]. Furthermore, CO_2 reduction reactions are multi-electron transfer processes driven without sacrificial agents, leading to complicated pathways, and different product types. Nevertheless, an analysis of the whole photocatalytic reduction processes is still missing. Therefore, it is necessary to establish a comprehensive model for conducting the efficiency assessment of the water-based photocatalytic CO_2 reduction system.

The surface redox reaction is crucial to the whole photocatalytic process. The determination of surface reaction rate is based on reaction product types and reaction mechanisms. There are a great variety of CO_2 reduction products including methanol (CH_3OH) [27], carbon monoxide (CO) [28], methane (CH_4) [29], and so forth. Among all products, CH_3OH is called the new fuel of the 21st century on account of its high energy density and high security and is used as raw material in chemical production widely [30]. Subsequently, CH_3OH is chosen as the reaction product. The reaction routine of CO_2 to CH_3OH is complicated, and there have been several reaction pathways proposed so far including the formaldehyde pathway, the carbene pathway, and the glyoxal pathway [31], [32], [33], [34].

2. Experimental method

The mechanisms of photocatalysts prepared by surfactants are complex and it is generally believed that due to the non-covalent interactions, such as hydrogen bonding, ð-ð interaction, and van der Waals interaction, between the surfactant and solid material, the surfactant was adsorbed on the surface of the solid material, inducing the material to self-assemble. Surfactant-assisted photocatalysts have been synthesized through various techniques, which mainly include sol-gel method, hydrothermal method, solvothermal method, emulsion method, and sonochemical method, etc. Among them, the most common synthesis methods are the sol-gel method, hydrothermal method, and solvothermal method. The sol-gel and hydrothermal methods are used in an aqueous media, whereas the solvothermal employs a non-aqueous media for the reaction.

2. Synthesis method

2.1.1 Sol-gel method

The sol-gel method has the advantages of high stability, short soaking times, low reaction temperature, and high purity of products, and it is considered to be one of the most promising methods for synthetic photocatalysts. In addition, the photocatalyst particles prepared by the sol-gel process generally have a narrow and uniform distribution and thermal stability. Therefore, the sol-gel method has attracted much attention in the preparation of porous photocatalysts [35]. This approach has been successful in the controllable design of multi-dimensional photocatalysts, such as pellets, fibers, films, and blocks. The chemical reactions involved in the sol-gel process are based on inorganic polymerization. As shown in Figure 1, the preparation process of the method is divided into three steps, namely hydrolysis, polymerization, and gel drying.

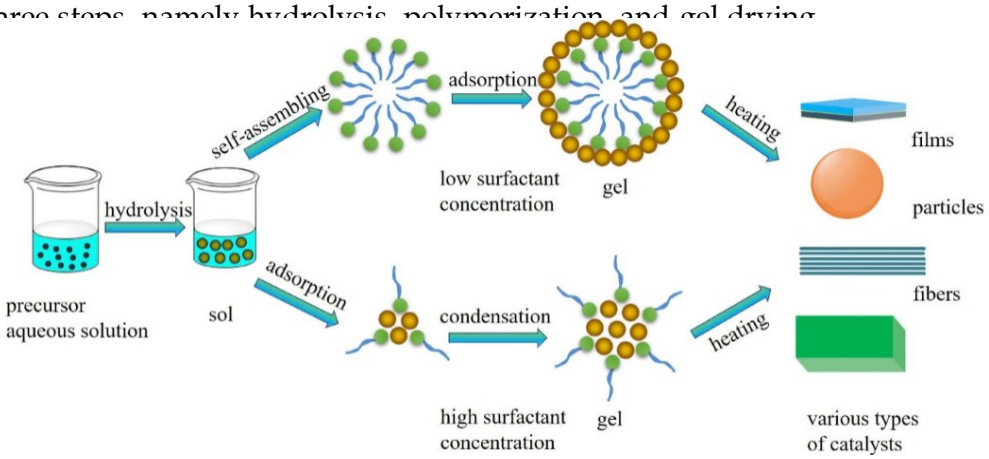

Figure 1. The possible preparation process of surfactant-assisted photocatalysts by sol-gel method.

Firstly, a solution of the precursor molecules needs to be hydrolyzed. The precursor is typically a metal organic compound such as an alkoxide, a chelated alkoxide or a metal salt. After hydrolysis, a suspension of colloidal particles (sol) is formed. Secondly, a large amount of water is present in the sol, and during the gelation process, the system loses fluidity and forms an open skeleton structure (gel). Finally, the gel is calcined to remove the surfactant to obtain the final photocatalyst [36], [37].

2.1.2 Hydrothermal method

Compared with other crystal preparation methods, the photocatalysts prepared by the hydrothermal method have the advantages of good grain development, small particle size, uniform distribution, and low-cost raw photocatalysts. In particular, they have the unique advantages of high crystallinity and morphology control [38]. The hydrothermal method has been successful in the controllable design of multi-dimensional photocatalysts, such as 1D photocatalysts (nanowires, nanobelts, nanotubes), hollow and thin films. In general, the hydrothermal method uses water as a solvent, and the sample needs to be dissolved and recrystallized firstly [39]. The possible preparation process of the hollow structure is shown in Figure 2. The sample is mixed in a solution and the reaction is carried out at a certain temperature. During the period, due to the presence of the surfactant, the samples self-assemble to form fine particles, and as the crystal grains grow up, the final morphology products are obtained.

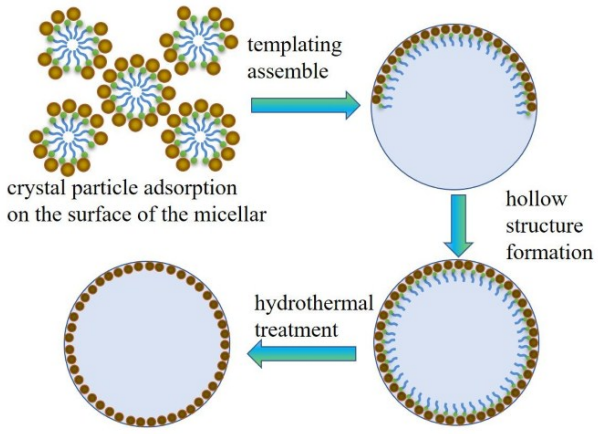

Figure 2. The possible preparation process of hollow photocatalysts by hydrothermal method.

2.1.3 Solvothermal method

The solvothermal method is developed on the basis of the hydrothermal method, using an organic or non-aqueous solvent as a solvent and the mixture reacting at a certain temperature [40], [41]. Compared with the hydrothermal method, the solvothermal method uses a non-aqueous solvent, which expands the range of solvent-based raw materials [42].

It is worth noting that, unlike the sol-gel and hydrothermal methods, the process of solvothermal preparation of photocatalysts is mainly divided into nucleation, dissolution, recrystallization, and growth, as shown in Figure 3.

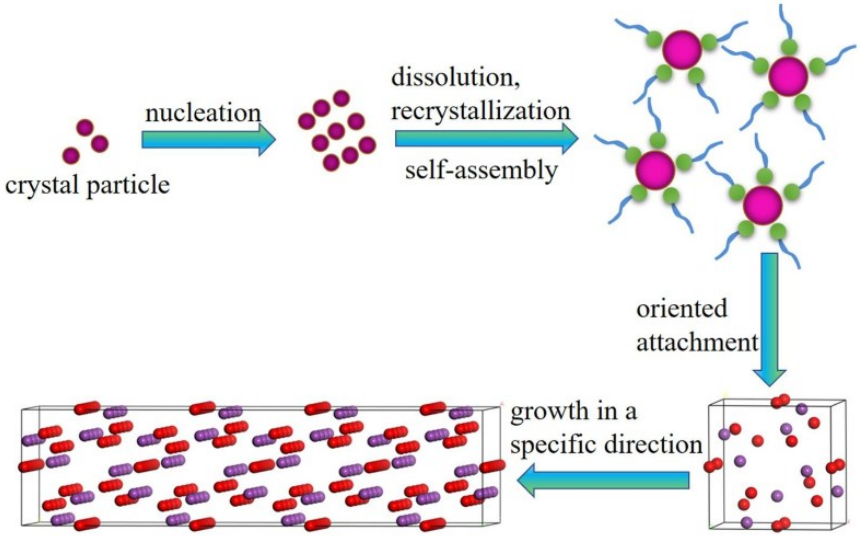

Figure 3. The possible preparation process of surfactant-assisted photocatalysts by solvothermal method.

2.1.4 Sonochemical method

The sonochemical method is a method of accelerating chemical reactions using ultrasonic waves. The sonochemical reaction is mainly caused by acoustic cavitation – the formation, oscillation, growth, shrinkage, and collapse of liquid hollow bubbles. This method has become an important tool for the production of novel nano-sized materials under ambient conditions in synthetic chemistry [43], [44].

2.1.5 Emulsion method

The emulsion polymerization method is a method in which a monomer is dispersed in water by an emulsifier and mechanical stirring to form an emulsion, and an initiator is added to initiate the polymerization of the monomer. The emulsion polymerization has the characteristics of high polymerization speed, high reaction conversion rate, low viscosity, stable dispersion system, and easy control. However, the separation and precipitation process of the polymer obtained by the emulsion polymerization method is complicated, and a demulsifier or a coagulant is added so that there are many residual impurities in the product [45, 46]. The polymerization mechanism can be divided into four stages: dispersion stage, aggregation stage, growth stage, and polymerization completion stage. The possible synthesis process of the emulsion polymerization process is shown in Figure 4.

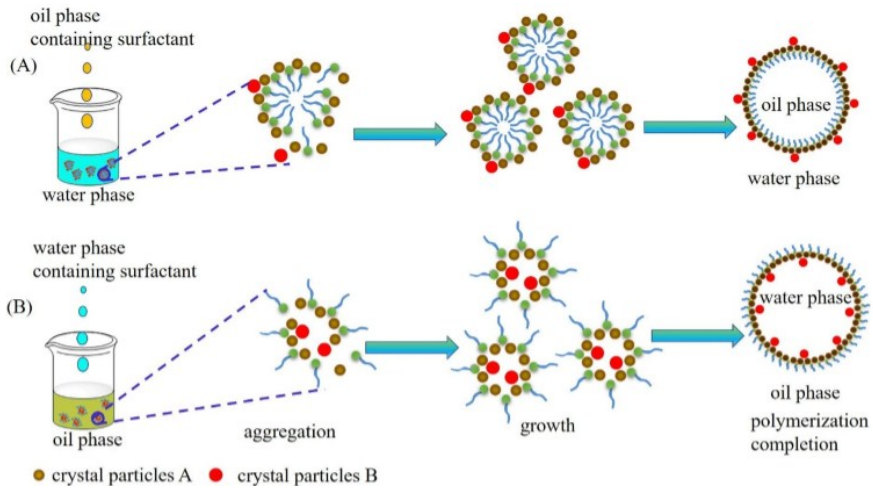

Figure 4. The possible preparation process of surfactant-assisted photocatalysts by emulsion (A) water-in-oil, (B) oil-in-water polymerization method.

2.1.6 Pechini method

The Pechini method has been widely used in the synthesis of oxide nanocrystals. The method is based on an intensive blending of positive ions in a solution, controlled transformation of the solution into a polymer gel, removal of the polymer matrix and

development of an oxide precursor with a high degree of homogeneity. When compared to other methods, the Pechini method has better compositional homogeneity, lower toxicity and lower cost [47]. The Pechini method stands out among several chemical synthesis methods because it allows for the use of different temperatures and proportions of citric acid and metallic cations, enabling controlled particle and/or agglomerate stoichiometry and morphology, compositional homogeneity, and low toxicity to produce a monophasic nanometric powder [48]. In the Pechini method the reaction is hydrolytic and produces a polymer which, after calcination, forms an oxide. The Pechini process involves two basic chemical reactions: the formation of a chelate complex consisting of carboxylic acid, chelating agent, and metallic matrix, followed by its polyesterification with an excess of polyalcohol (as shown in Figure 5). The reactants usually employed in this application are citric acid and glycol ethylene.

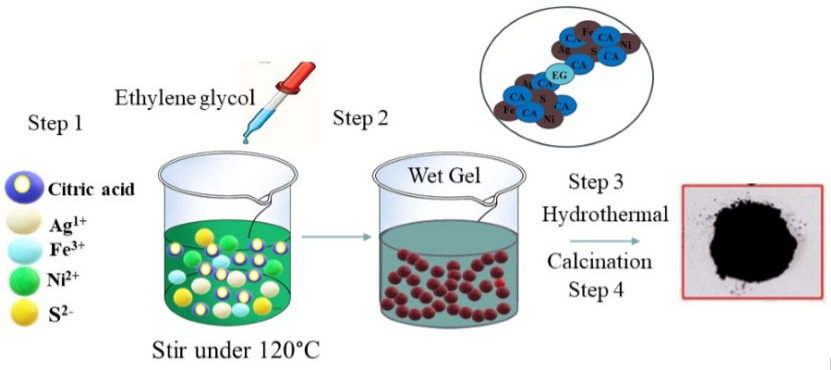

Figure 5. The possible preparation process of Pechini method.

2.2 *Photocatalyst for the CO_2 reduction*

A number of strategies have been developed and implemented by engineering their structures at different scales so as to promote their efficiency in light absorption, charge separation and interfacial charge transfer.

2.2.1. Metal Oxide

Metal oxides are a very common type of photocatalyst materials for CO_2 reduction. A large number of them consist of transition metal cations (e.g., Ti^{4+}, Zr^{4+}, Nb^{5+}, Ta^{5+}, W^{6+}, and Mo^{6+}) with the d^0 configuration. Their conduction bands are composed of vacant metal *d* orbitals and usually more negative than 0 V, while their valence bands are composed of O_{2p} orbitals and usually more positive than 3 eV [49]. The band structure of these metal oxides can generally enable the simultaneous CO_2 reduction and water oxidation, but their wide band gap more than often restricts the utilization of solar spectrum only within the UV region. TiO_2 is the most representative and well

studied d^0 metal oxide semiconductor photocatalyst with the advantages of low cost, low toxicity, and chemical stability [50]. Among its three polymorphs that naturally exist, the anatase form of TiO_2 receives wide attention and is shown to be highly active in photocatalytic CO_2 reduction. Comparatively, rutile is less active due to its fast charge recombination, and brookite, on the other hand, is rarely investigated for photocatalysis probably due to the past difficulty in obtaining phase pure brookite (Figure 6).

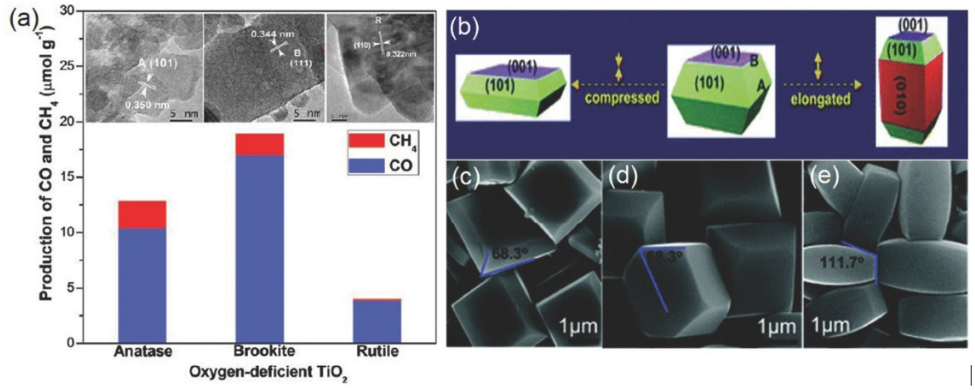

Figure 6. a) Production rates of CO and CH_4 on three TiO_2 nanocrystal polymorphs (anatase, rutile, and brookite). b) Schematic of anatase TiO_2 with different percentages of {101}, {001}, and {010} facets and c–e) SEM images of corresponding synthetic products [50, 51].

2.2.2. *Metal sulfide*

Metal sulfides represent another large group of photocatalyst materials for CO_2 reduction. Compared to their oxide counterparts, metal sulfides possess higher valence bands mainly of the S 3p character and have narrower band gaps. It is, however, a general concern that photogenerated holes on their valance band may not be energetic enough to oxidize water and would instead result in their irreversible photo corrosion. As a result, hole scavengers are frequently added in order to extend their stability [52].

2.2.3. *Metal nitride*

Metal nitrides or oxynitrides also have narrow band gaps due to their high valence bands mainly composed of N 2p orbitals. Despite their desirable visible light absorbance, little photocatalytic activity, however, was generally observed for d^0 transition metal nitrides and oxynitrides such as Ta_3N_5, TaON, $MTaO_2N$ (M = Ca, Sr, Ba and La) probably due to their low conduction band edge. It is suggested that d^{10} metal with broadly dispersed conduction bands are more promising toward photocatalytic CO_2 reduction [53].

2.2.4. *Layered Double Hydroxide (LDH)*

LDH with the general formula of $[M^{2+}_{1-x}M^{3+}_{x}(OH)_2][A^{n-}_{x/n}\cdot mH_2O]$ (where M^{2+}, M^{3+}, and A^{n-} are divalent cation, trivalent cation, and interlayer anion, respectively) is a class of layered materials comprising positively charged metal hydroxide layers and charge

balancing anions between the layers. Many LDH compounds (such as Ti based LDHs) are known to be excellent photocatalysts for water splitting. Their potential in photocatalytic CO_2 reduction was first uncovered by Izumi's group in 2011. Up to now, LDHs containing Zn^{2+}, Cu^{2+}, Mg^{2+}, and Ni^{2+} combined with Al^{3+}, Ga^{3+}, Cr^{3+}, and In^{3+} are shown to be active for reducing CO_2 to CO or methanol as main products [54]. Inclusion of Cu ions within the host layers or replacing the interlayer anions with cuprous anions generally improves the selectivity for methanol over CO production

2.2.5. Metal-organic framework (MOF)

MOFs are a family of porous materials with crystalline and open structures consisting of metal ions or clusters coordinated with organic ligands [55]. Since both the organic ligands and metal ions can be systematically varied, MOFs possess extraordinary chemical and functional versatility. Most uniquely, they may contain photosensitizers and catalytic centers in a single solid, and thereby represent promising alternatives to conventional semiconductors for photocatalysis. For example, many Ti-based MOFs combine the photocatalytic activity of titanium oxide clusters with the light adsorbing properties of organic linkers and are photo catalytically active under UV–vis light. Li and co-workers first reported Ti containing MIL-125-NH_2 with the 2-aminoterephthalate linker as the photocatalyst for CO_2 reduction to formate under visible light irradiation.

2.2.6. Metal-free material

Graphene is a 2D structured sp^2-hybridized carbon material in a honeycomb structured. Graphene has many profitable properties, such as mechanical strength [45], molecular barrier ability. In addition, the procedure of graphene has categorized in two groups: (i) top to down method-synthesized by etching out crystal planes (mechanical exfoliation, oxidation–reduction, liquid phase exfoliation), (ii) bottom to up method-synthesized by the atoms stick onto the substrates which gives rise to crystal planes (chemical vapor deposition, epitaxial growth). There are four routes for synthesis of graphene which include those of Brodie, Staudenmaier, Hofmann and Hummers. Currently, the Hummers method is widely used as it is a fast and safety method. Carbon materials combined with semiconductor, which including a graphite, carbon black, activated carbon, carbon fibers, carbon nanotubes (CNTs), and fullerenes. Furthermore, the unique two-dimensional planar structure and high specific surface of GR mean that it shows great potential as a carrier and multifunctional material for transferring electrons and holes. The mechanism of enhancement of photocatalysis by Graphene: semiconductors possess a low-energy VB which has a full of electrons, a high-energy CB which has an empty orbital and has a bandgap difference between two band state.

2.3. Electrocatalytic material for the CO_2 reduction

2.3.1. Metals

Elemental metals are among the earliest investigated CO_2RR electrocatalysts. In a series

of seminal works published between 1980s and 1990s, Hori et al. first reported that CO, CH_4, formate, and other hydrocarbons were detected from the electrocatalytic CO_2RR on various metal electrodes in aqueous $KHCO_3$ electrolyte solution [56-58]. Based on the reduction products, these metals are divided to three groups. The first group includes Sn, Pb, Bi, In, etc. They hardly adsorb the $CO_2^{\bullet-}$ intermediate. Desorbed $CO_2^{\bullet-}$ tends to be protonated at the carbon atom and ultimately transforms to formate or formic acid as the major reduction product. The second group includes Au, Ag, Zn, Pd, Ga, etc. They can bind the $CO_2^{\bullet-}$ intermediate, catalyze the cleavage of C?O bond in CO_2, and allow resultant CO to easily desorb from the electrode as the major reduction product. The third group includes Pt, Ti, Ni, Fe, etc. They have low HER overpotentials and strong CO adsorption properties, giving rise to H_2 as the major production. In addition to the three groups, Cu is the only elemental metal capable of producing C_1–C_3 hydrocarbons at significant rates. It is suggested that the adsorption of CO on Cu is suitable for its further reduction to hydrocarbons or alcohols at high overpotentials through COH or CHO intermediates. Theoretical simulation has been proven a powerful tool to understand the electrocatalytic CO_2RR activity and selectivity on different metals. Nørskov and co workers used density functional theory (DFT) calculations to describe trends in catalytic activity for CO_2 reduction to CO as a function of the adsorption energies of the two reaction intermediates—COOH and CO.

2.3.2. Metal chalcogenides

Layered transition metal dichalcogenides (TMD) such as MoS_2, $MoSe_2$, and WS_2 have been widely investigated as the HER electrocatalysts. However, it is not until recent years that their potential in CO_2RR starts to be unveiled. Nørskov and co workers used DFT calculations to explore the binding properties of CO_2RR intermediates (COOH, CHO, and CO) on MoS_2 and $MoSe_2$ edges [59]. COOH and CHO were found to prefer bridging S or Se atoms, while CO was selectively adsorbed on the metal atom. These authors argued that in this way, the active edges may break the scaling relations observed between intermediates on transition metals, making them potentially more attractive for CO_2RR than even the best transition metals. Because TMD materials are excellent HER electrocatalysts, CO_2RR of TMD materials usually have to be carried out in mixture solution of ionic liquid (e.g., EMIM BF_4) and water in order to suppress HER. Some ionic liquids are reported to form a stable complex with the $CO_2^{\bullet-}$ intermediate so that they can lower the activation energy barrier for effective CO_2 reduction.

2.3.3. Carbonaceous materials

Carbonaceous materials are also applied for CO_2RR electrocatalysis by virtue of their good electrical conductivity, low cost, chemical stability and usually large surface area. However, pristine carbonaceous materials are generally inert and have negligible activity for CO_2RR because they can hardly activate CO_2 molecule or adsorb $CO_2^{\bullet-}$ intermediate [60, 61]. It is a different scenario when carbonaceous materials are properly doped with heteroatoms (e.g., N, B, P, and S). Doping introduces structural defects or induces charge/

spin densities on the adjacent carbon atoms, therefore significantly altering the interaction between carbonaceous materials and CO_2 or reaction intermediates.

2.4. Experimental part of CO_2 reduction

The photocatalytic CO_2 reduction in aqueous media has sparked a huge interest because of reactants availability, low cost, system simplicity, etc. However, the performance of this photocatalytic system is too sluggish to meet the efficiency requirement of industrial commercialization. In the reduction of CO_2, the water used as a as the hole scavenger, ranging from the exploration of novel catalysts , bandgap engineering, recombination inhibition , to system optimization. In detail, The photocatalytic reduction of CO_2 was examined in a three-part reactor (Figure 6), using the 500-W metal halide lamp as the light source. In detail, 100 mg of the photocatalyst with two different sacrificial scavengers were dispersed into 0.04 M $NaHCO_3$ containing 50 ml solvent and stirred it for 1 h, filled the reactor with pure CO_2 gas for 30 min, and turned on the light. After 48h of reaction, we withdrew the different amounts of final samples using a syringe and membrane filter, which were 0.45 ìm in pore size and 47 mm in diameter, respectively, from the reactor every 12 h. The final samples by a "Quantitative analysis of alcohol" method. In alcohol analysis, 10 ml of 0.1 M CrO_3 added into 1-ml sample and agitated it for 15 min, then centrifuged the suspension (10.000 ppm/15 min). The concentration of acquired solution examined by a UV spectrophotometer (Optizen POP, Korea) using a quartz cell (1 cm × 4.5 cm) [62].

The electrochemical CO_2 reduction process was conducted on a PGP201 Potentiostatic (A41A009) using a three-electrode system. Ag/AgCl and platinum were used as the reference and counter electrode, respectively. The as-prepared binary and ternary nanocomposites were used for the working electrode (WE) preparation. The WE were prepared by following the "Doctor blade" method [63]. Ethyl cellulose was used as a binding material and mixed with the as-prepared nanocomposite in a 1:3 ratio. Then, a few drops of pure ethanol were added, and the resulting mixture was ground and used to veneer the top of the Ni foil. The electrode preparation process is presented in Scheme S2. The current density determines the amount of electric current per unit cross-section of the material. The input CO_2 gas-purging speed and the amount of gas were controlled by the mass-flow controller and 50 ml of 0.04 M $NaHCO_3$ solvent was used as the electrolyte solution. The cyclic voltammetry (CV) measurement was conducted in a potential range of (-1.2 to 1.5 V vs. Ag/AgCl) at a scan rate of 100 mV s^{-1}. After electrolysis, a voltammogram was obtained for the final product cycle considering the highest oxidation peak current. In a reaction that reduces the electrochemical composition of CO_2, the catalyst can direct a specific reaction to produce a certain amount of product. In CO_2RR, the following equation considers the Faraday efficiency (FE) to confirm the selected product during the reaction [64].

$$FE\% = \frac{n_{methanol} \times n \times F}{\int_0^t Idt} \times 100$$

where, $n_{methanol}$ is the number of moles of formate and n represents the number of electrons transferred from CO_2 to produce one molecule of methanol. In this case, n = 6, F is Faraday's constant (96,485 C mol^{-1} of electrons), and I is the circuit current (measured by the Potentiostatic). Reaction time (t) is measured in s.

3. Result and discussion

Elemental metals are among the earliest investigated CO_2RR electrocatalyst. Based on the obtained product, the studied metals are classified into three groups, and due to the physical properties of the metal, the reduction of the CO_2 can be changed. Cu is the only known elemental metal that can reduce CO_2 beyond CO or formic acid. In addition to the two electron reduction products, methane, ethane, ethylene, ethyne, methanol, and ethanol are all measured as the possible reduction products. Recent work by Jaramillo and co-workers reported the identification of 16 different reduction products on metallic Cu surface (Figure 7a). Aside from common products, some aldehydes, ketones, carboxylic acids, esters, and hydrocarbons such as paraffins and olefins containing up to six carbon atoms could also be generated as minor products on Cu electrocatalysts. It was proposed that these Ce^{-2} products might be formed via enol like surface intermediates. Nevertheless, deep reduction of CO_2 is kinetically challenging: these higher value chemicals generally cannot be produced at significant rates until at very negative potentials (-0.8 V vs reversible hydrogen electrode or RHE) and their Faradaic efficiency is usually <30%.

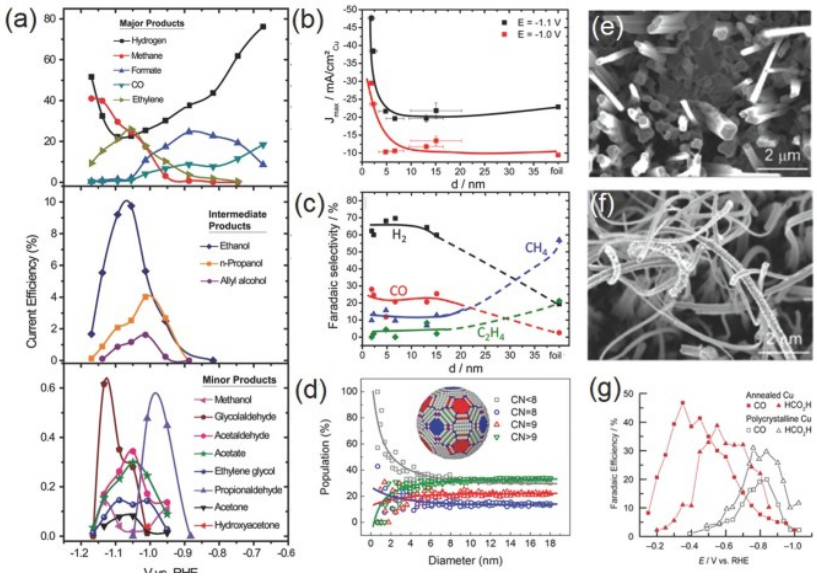

Figure 7. a) Faradaic efficiency as a function of potential for major (top), intermediate range (middle), and minor (bottom) products on a metallic Cu surface. Particle size dependence of b) current density and c) Faradaic efficiency for different CO_2RR products on Cu NPs; d) population of surface atoms with certain coordination number (CN) as a function of particle diameter. Scanning electron microscope (SEM) images of e) an annealed Cu electrode and f) the same electrode after CO_2RR; g) Faradaic efficiency for CO and HCOOH as a function of potential on polycrystalline Cu and annealed Cu [65, 66].

To promote the electrocatalytic performance of Cu, different strategies have been exploited. The morphology of Cu catalysts has a profound influence on the catalytic activity and product selectivity. On single crystal Cu electrodes, the selectivity toward hydrocarbons (mainly methane and ethylene) is strongly dependent on the electrode surface. Hori et al. first showed that ethylene formation was favored on Cu (100) surface, whereas methane was the main hydrocarbon product on Cu (111) terraces. Particle size is also an important structural parameter for Cu-based CO_2RR electrocatalysts. Strasser and co workers discovered that Cu nanoparticles (NPs) exhibited dramatically enhanced total current density and higher selectivity toward CO and H_2 as their particle size was decreased, particularly for those under 5 nm, while hydrocarbon selectivity was increasingly suppressed (Figure 7b–d) [65]. This experimental observation was rationalized by DFT calculations, which showed that smaller Cu NPs could provide more undercoordinated atoms as strong binding sites to key intermediates such as H and COOH, thus accelerating HER and the reduction of CO_2 to CO while decreasing further recombination reaction to hydrocarbons. However, conflicting results were also disclosed by Alivisatos and co workers showing that Cu NPs ($\approx$ 7 nm, grew to $\approx$ 25 nm during electrochemical experiments) exhibited an enhanced methanation current density four times greater than that of Cu foil, and an average Faradaic efficiency of 80% during extended electrolysis [66]. The marked difference in reaction selectivity might be caused by the different synthetic approaches and measurement conditions employed.

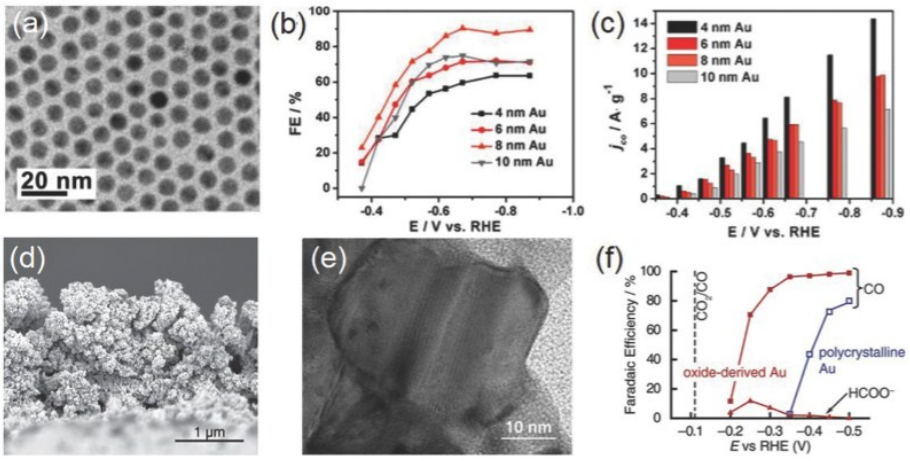

Figure 8. a) Transmission electron microscopy (TEM) image of 8 nm Au NPs; b) potential dependent Faradaic efficiency for CO on Au NPs with different sizes; c) current densities for CO formation at various potentials. d) Cross sectional SEM image and e) high magnification TEM image of oxide derived Au NPs; f) Faradaic efficiency for CO and formate on oxide derived Au NPs in 0.5 M $NaHCO_3$ [67].

Like Cu NPs, the reaction activity and selectivity of Au NPs strongly depends on their particle size. Smaller NPs are not necessarily more desirable for electrocatalytic CO_2RR. Sun and co workers prepared monodispersed Au NPs having diameters of 4, 6, 8, and 10 nm and found that the 8 nm Au NPs exhibited the optimal activity and Faradaic efficiency for CO (90% at -0.67 V vs RHE) (Figure 8a–c) [67]. DFT calculations disclosed

that edge sites on the Au NP surface facilitated CO formation by stabilizing key intermediates such as COOH while the corner sites were active for HER owing to their increased affinity toward H. The highest selectivity observed with 8 nm Au NPs was attributed to their optimal ratio of edge sites over corner sites. Similar size dependence was also reported by Cuenya and co workers for Au NPs of 1–8 nm. As the NP size decreased, the authors observed a dramatic increase in current density and a significant decline in CO selectivity. It was rationalized by the increasing low coordinated sites that were suggested to favor HER over CO_2 reduction.

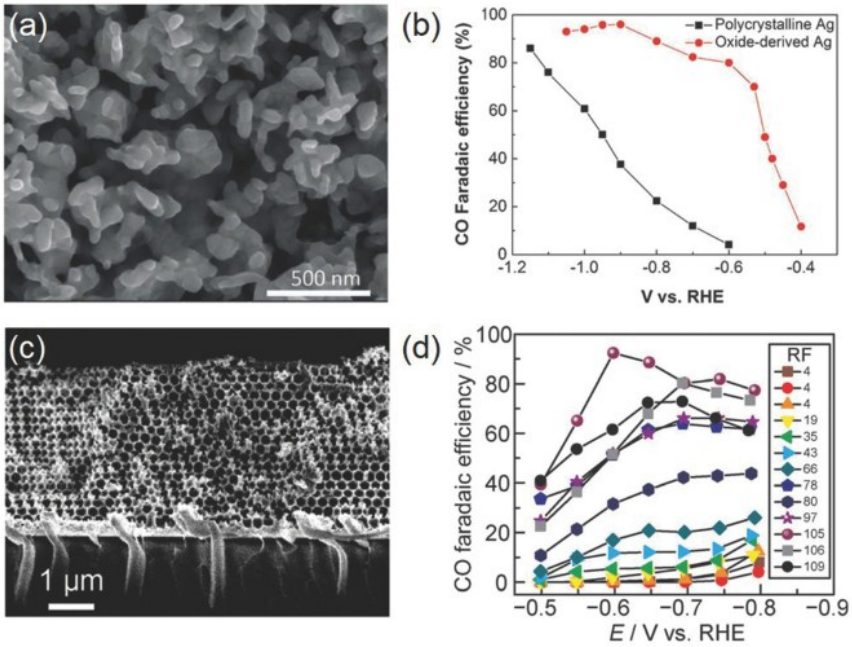

Figure 9. a) SEM image of oxide derived Ag; b) Faradaic efficiency for CO on polycrystalline Ag and oxide-derived Ag. c) Cross sectional SEM image of an Ag IO film; d) potential dependent Faradaic efficiency for CO on Ag films with varying roughness factors [68, 69].

Ag is the second noble metal that can enable the highly selective reduction of CO_2 to CO, but it is relatively less active than Au due to its intrinsically weaker binding toward reaction intermediates [68]. For bulk Ag metal, Hori and co workers found that the electrocatalytic activity of CO_2 reduction to CO was substantially faster on atomically stepped Ag (110) than that on flat Ag (100) or Ag (111). Nanostructured Ag is considerably more attractive than bulk Ag metal for CO_2RR. Studies on Ag NPs by Masel and co-workers showed an increasing CO_2RR current density as their size decreased from 200 to 5 nm [69]. However, the current density significantly dropped if the size further decreased to 1 nm. Smith and co workers reported that the oxide derived Ag electrode from the anodization of Ag foil in alkaline solutions had a highly porous structure (Figure 9 a,b). It attained H"80% Faradaic efficiency for reducing CO_2 to CO at a moderate overpotential of 0.49 V, much enhanced than untreated polycrystalline Ag (H"4%) under identical conditions. This improvement was likely correlated with the nanostructured surface populated with highly active sites for stabilizing COOH

intermediate as well as a high local pH arising from porosity induced transport limitation. A nanoporous silver was synthesized by Jiao and co workers from two-step dealloying of an Ag Al precursor.

Layered transition metal dichalcogenides (TMD) such as MoS_2, $MoSe_2$, and WS_2 have been widely investigated as the HER electrocatalysts [70]. In 2014, Salehi Khojin and co workers first experimentally demonstrated bulk MoS_2 as a highly efficient electrocatalyst for selectively reducing CO_2 to CO with a small overpotential of 54 mV in a mixture of 96 mol% water and 4 mol% EMIM BF_4 [71]. An impressive cathodic current density of $\approx$ 65 mA cm^{-2} and a CO Faradaic efficient of 98% were delivered at η = 0.65 V, much improved than Au and Ag NPs. At η = 54 mV, it exhibited an exceptional current density of $\approx$ 19 mA cm^{-2}, CO Faradaic efficiency of 24%, and TOF of 0.28 s^{-1} in 50:50 vol% ionic liquid/water electrolyte; at η = 0.65 V, the recorded current density for WSe_2 reached 330 mA cm^{-2} with a Faradaic efficiency of $\approx$ 85%—an unprecedented activity surpassing any other known CO_2RR electrocatalysts (Figure 10).

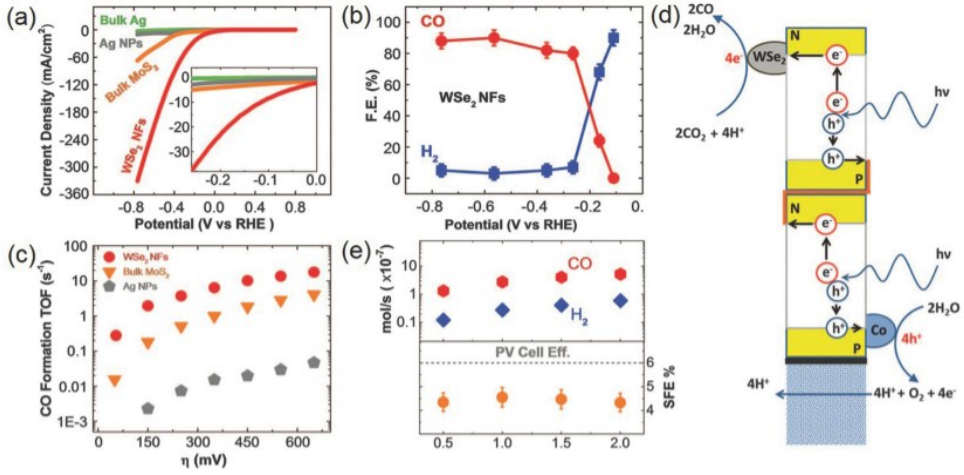

Figure 10.a) CV curves of WSe_2 NFs, bulk MoS_2, Ag NPs, and bulk Ag in CO_2 saturated EMIM BF_4/H_2O solution; b) potential dependent Faradaic efficiency for CO and H_2 on WSe_2 NFs; c) CO formation TOF of WSe_2 NFs, bulk MoS_2, and Ag NPs; d) schematic showing an artificial leaf with WSe_2 cocatalyst for reducing CO_2 to CO under light illumination. e) Product formation rates under different light illumination intensities using the WSe_2/IL cocatalyst system [70].

In recent years, the great potentials of 2D nanostructures such as nanosheets or nanoflakes start to be gradually unveiled. These 2D materials often have high specific surface areas that can provide abundant active sites for the CO_2 adsorption and photocatalytic reaction. Xie and co workers developed a series of 2D atomic thick semiconductor materials for photocatalytic CO_2 reduction. Ye and co workers prepared ultrathin $W_{18}O_{49}$ nanowires with diameter below 1 nm (Figure 11a) [72]. They showed strong light absorption from the visible to the near infrared region and was able to reduce CO_2 to CH_4 in the absence of any cocatalyst at an impressive formation rate of 666 ppm g^{-1} h^{-1}. Zou and co workers prepared single crystalline Zn_2GeO_4 nanobelts that was featured with thickness as small as $\approx$ 7 nm and aspect ratio up to 10 000

(Figure 11b,c). Their high crystallinity and ultralong/ultrathin geometry configuration facilitated the migration and separation of photogenerated carriers and consequently resulted in an improved photocatalytic activity for reducing CO_2 to CH_4.

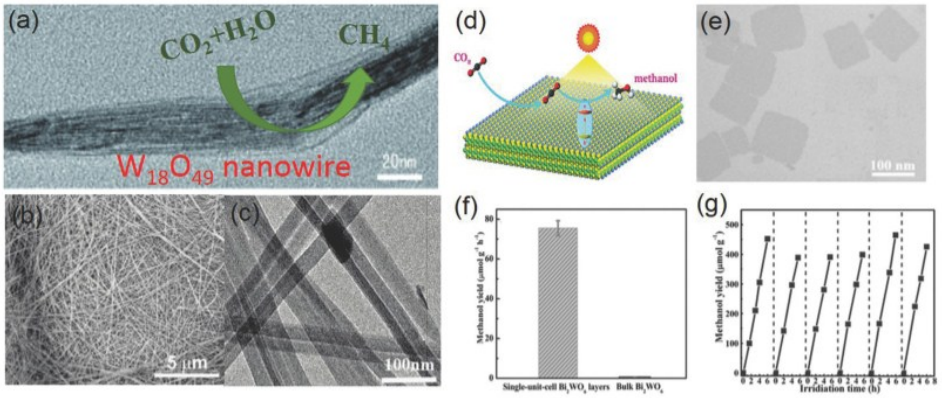

Figure 11. a) TEM image of $W_{18}O_{49}$ nanowires for selectively reducing CO_2 to CH_4. SEM and TEM images of Zn_2GeO_4 nanoribbons. d) Schematic of the photocatalytic CO_2 reduction to methanol on the single unit cell Bi_2WO_6 layers; e) TEM image of Bi_2WO_6 layers; f) methanol formation rate on Bi_2WO_6 layers and bulk Bi_2WO_6, g) stability of methanol formation on Bi_2WO_6 layers [72].

Ye and co-workers reported that the co-doping of mesoporous TiO_2 altered both its CB and VB structure and increased its visible light absorption [73]. The main CO_2 reduction products were CO and CH_4, and their selectivity could be tuned by adjusting the Co doping level. An optimal activity of 90 μmol g^{-1} h^{-1} for CH_4 and 1.94 mmol g^{-1} h^{-1} for CO was achieved at the Co/Ti molar ratio of 2.5%. Compared to cation doping, anion doping is even more desirable. This is because for most oxides (e.g., TiO_2, ZrO_2, Nb_2O_5, and In_2O_3), there is a large room for raising their VB edges without compromising their capability to oxidize water. Partially replacing O in the lattice with other nonmetal elements such as B, C, N, S, and P is proven effective (Figure 12a). Additional electronic states above the valence band edge introduced by the nonmetal doping were found responsible for the visible-light response as corroborated by DFT calculations (Figure 12b) and X-ray photoelectron spectroscopy characterizations.

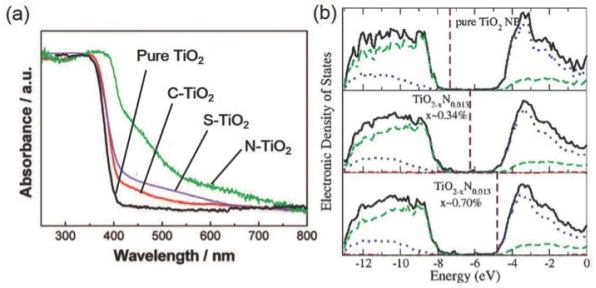

Figure 12. a) Diffuse reflectance spectra of pure TiO_2, C doped TiO_2, S doped TiO_2, and N doped TiO_2 showing the prominent effect of anion doping. b) Calculated density of state (DOS) of pure TiO_2 and N doped TiO_2 with different concentrations of O vacancies [73].

Engineering the type and density of defects on catalyst surfaces is an important means to tune their activities. Oxygen vacancies are among the most common defects in oxide or hydroxide surfaces and are suggested to greatly affect the photocatalytic CO_2 reduction. Among many experimental supports was the low temperature scanning tunneling microscopy visualizing that CO_2 molecules were preferably absorbed at the oxygen vacancies (Figure 13a) [74]. Quantum mechanical modeling also indicated that the electron transfer from the CB of stoichiometric anatase TiO_2 to CO_2 was not energetically favorable, but defects on anatase TiO_2 surface could promote the electron transfer to CO_2. Zhang and co workers recently reported that abundant oxygen vacancies and coordinatively unsaturated Zn^+ centers were created when the thickness of ZnAl LDH nanosheets were reduced to two repeat stacking layers (Figure 13b–d). Thus formed Zn^+ V_o complexes served as the active sites for the efficient adsorption of CO_2 and H_2O molecules, significantly improving the photocatalytic activity for CO_2 reduction to CO.

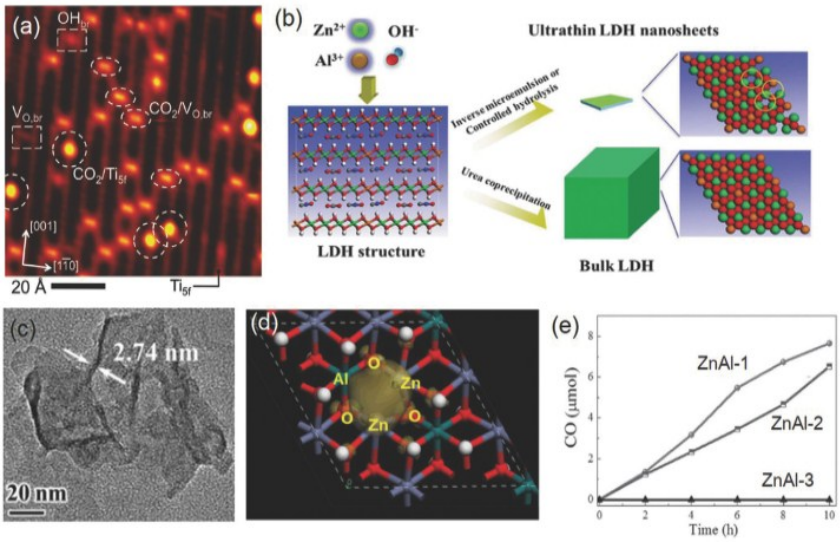

Figure 13. a) Scanning tunneling microscope (STM) image of CO_2 molecules adsorbed on TiO_2 (110) plane. b) Schematic showing the formation of coordinatively unsaturated ZnAl-LDH nanosheets; c) TEM image of coordinatively unsaturated ZnAl-LDH nanosheets; d) charge density distribution for the valence band maximum of V_o-doped ZnAl-LDH; e) time dependent CO yields on different ZnAl-LDH samples [74].

As shown in in Figure 14a, the type II of heterostructure is the most desirable since it promotes the spatial charge separation by transferring electrons to one material with the lower CB and holes to another material with the higher VB. Coupling semiconductors with staggered gaps is an approach frequently adopted in photocatalysis. TiO_2 is a common component of many heterostructures. Dong and co workers described a hierarchical assembly of ultrathin $ZnIn_2S_4$ nanosheets on TiO_2 electrospun nanofibers (Figure 14b–d) [75]. The optimal photocatalyst achieved a total CH_4 evolution rate of 10.92 μmol g^{-1} h^{-1}, which were 34.1 and 4.2 times higher than individual AgBr and pCN respectively due to the improved separation efficiency of photogenerated electron/hole pairs at the heterojunction interface.

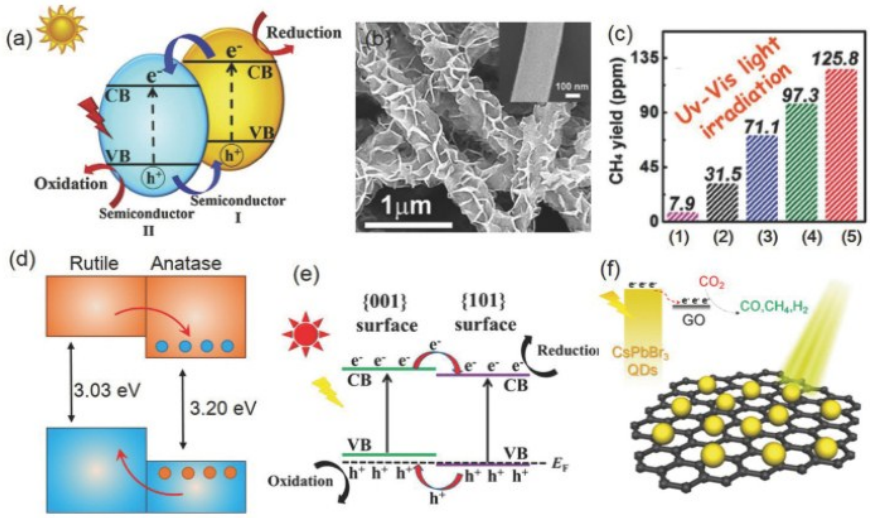

Figure 14. a) Schematic of the conventional type II heterojunction photocatalyst. b) SEM image of $ZnIn_2S_4$/TiO_2; c) comparison of CH_4 yield from photocatalytic CO_2 reduction on 1) $ZnIn_2S_4$, 2) TiO_2, 3) $ZnIn_2S_4/TiO_2$, 4) $Au/ZnIn_2S_4/TiO_2$, and 5) $Ag/ZnIn_2S_4/TiO_2$ after UV–vis irradiation for 4 h. d) Proposed VB and CB alignment for the anatase/rutile interface. e) Schematic {001}/{101} surface heterojunction., f) Schematic of CO_2 photoreduction over the $CsPbBr_3$ QD/GO photocatalyst [75].

Noble metals including Pt, Au, Pd, and Ag represent the most widely used cocatalyst materials for photocatalytic CO_2 reduction. These noble metals can often serve as the electron sink to concentrate photogenerated electrons from photocatalysts, and consequently reduce the possibility of electron-hole recombination. The most effective cocatalyst was identified to be Pt, presumably due to its efficient extraction of photogenerated electrons from TiO_2. It was also recognized that the size of cocatalyst particles affected the photocatalytic activity and selectivity. CH_4 formation was more favored on smaller Pt nanoparticles. TiO_2 loaded with H"3 nm (mean size) Pt nanoparticles was measured to produce CH_4 about four times faster than TiO_2 loaded with H"5 nm Pt nanoparticles. The optimal particle size was measured to be H"1 nm. With such a cocatalyst particle size, a peak CH_4 formation rate of 1361 μmol g^{-1} h^{-1} was observed, and the corresponding quantum yield was calculated to be 2.41% (Figure 15a). By contrast, larger or smaller cocatalyst nanoparticles led to markedly reduced photocatalytic activity. The difference was rationalized based on the relative energy band alignment of TiO_2 and Pt as its size varied: too small Pt particle size would lift its energy level above the bottom of the TiO_2 CB due to the quantum confinement, retarding the electron transfer from photocatalyst to Pt cocatalyst, whilst for bigger Pt nanoparticles, their properties approached bulk Pt and could act as recombination centers by capturing both photogenerated electrons and holes. As previously mentioned, alloying of different metals offers the probability to tailor their electrocatalytic activity and selectivity. Garcia and co workers showed that Au–Cu nanoalloy cocatalyst greatly promoted the photocatalytic activity of commercial P25 TiO_2 (Figure 15b).

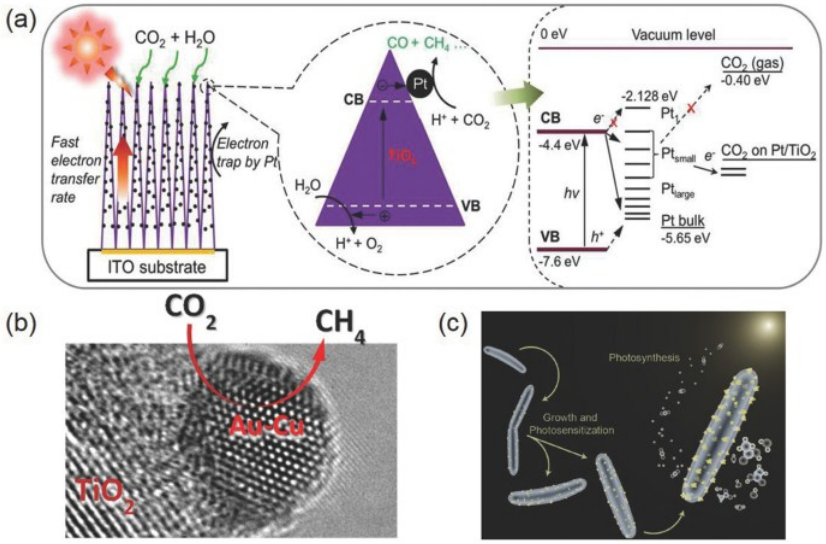

Figure 15. a) Schematic of photocatalytic CO_2 reduction on nanostructured TiO_2 films deposited with Pt cocatalyst particles of varying sizes. Different alignments between TiO_2 band structure and Pt work function are suggested to be responsible for the observed different photocatalytic activities. b) High resolution TEM image of an Au"Cu nanoparticle deposited on the TiO_2 surface as the cocatalyst for selectively reducing CO_2 to CH_4. c) Schematic showing the *M. thermoacetica*–CdS hybrid system for the photosynthetic conversion of CO_2 to acetic acid [76, 77].

4. Conclusion

In conclusion, the photocatalytic performance, crystal structure and charge transfer properties of the photocatalyst are depends on the synthesis method. The synthesis method is divided into 6 ways and each method has specific advantage side. The photocatalyst material highly used for the photocatalytic reduction of CO_2. Principle side of photocatalytic CO_2 reduction like thermodynamics, mass transfer, and selectivity and reaction mechanism have been deliberated. To further enhance the CO_2 reduction performance, improvements can be possibly made from the following two directions. Seeking new material compositions and structures would continue to be at the heart of electrocatalytic and photocatalytic CO_2 reduction research. For photocatalytic CO_2 reduction, the exploration of new materials and structures can also be greatly accelerated by borrowing knowledge from photocatalytic water splitting. Photocatalytic CO_2 reduction and photocatalytic water splitting only differs in their surface reaction step. If strategies (such as incorporation of proper cocatalysts) can be undertaken to significantly shift the cathodic reaction selectivity away from HER to CO_2RR, essentially all existing photocatalysts for water splitting can be transformed to those for CO_2 reduction. The efficiency of the photocatalytic reaction depends greatly on the efficiency of electron transfer and charge transfer from metal/metal oxide to graphene (carbon material). On the other hand, the photocatalytic carbon dioxide (CO_2) reduction in aqueous media provides a potential and convenient way for fulfilling increasing fossil energy demand and relieving global warming problems. In conclusion, the combination

of semiconductor with graphene, the charge transfer properties, bandgap, the recombination coefficient and the condition of reduction process are the main factors for the photocatalytic reduction of carbon dioxide. CO_2 electrochemical reduction is a process involving transfer of multiple electrons and protons. Because of the low solubility of CO_2 in electrolytes, how to deliver CO_2 effectively to the cathode surface becomes the key to achieve a high current density and a high CO_2 reduction selectivity simultaneously in a practical CO_2 electrolyzer.

Reference

1. P.M. Vitousek, H.A. Mooney, J. Lubchenco, J.M. Melillo, Human Domination of Earth's Eco systems, *Science* 1997, **277**, 494.
2. W.H. Wang, Y. Himeda, J.T. Muckerman, G.F. Manbeck, E. Fujita, CO_2 Hydrogenation to Formate and Methanol as an Alternative to Photo- and Electrochemical CO_2 Reduction, *Chem. Rev*. 2015, **115**, 12936.
3. National Ocean and Atmospheric Administration (NOAA), National Centers for Environmental Information, Global Climate Change Indicators.
4. M.I. Hoffert, K. Caldeira, G. Benford, D.R. Criswell, C. Green, H. Herzog, A.K. Jain, H. S. Kheshgi, K.S. Lackner, J.S. Lewis, Advanced Technology Paths to Global Climate Stability: Energy for a Greenhouse Planet, *Science* 2002, **298**, 981.
5. S.Y. Tee, K.Y. Win, W.S. Teo, L.D. Koh, S. Liu, C.P. Teng, M.Y. Han, Recent Progress in Energy Driven Water Splitting, *Adv. Sci*. 2017, **4**, 1600337.
6. Y. Hori, A. Murata, R. Takahashi, Formation of hydrocarbons in the electrochemical reduction of carbon dioxide at a copper electrode in aqueous solution, *J. Chem. Soc., Faraday Trans. 1* 1989, **85**, 2309.
7. R.J. Lim, M. Xie, M.A. Sk, J.M. Lee, A. Fisher, X. Wang, K.H. Lim, A review on the electrochemical reduction of CO_2 in fuel cells, metal electrodes and molecular catalysts, *Catal. Today* 2014, **233**, 169.
8. B. Hu, C. Guild, S.L. Suib, Thermal, electrochemical, and photochemical conversion of CO_2 to fuels and value-added products, *J. CO_2 Util.* 2013, **1**, 18.
9. M.E. Royer, Reduction of carbonic acid into formic acid, *Compt. Rend*. 1870, **70**, 731.
10. Y. Hori, K. Kikuchi, A. Murata, S. Suzuki, Production of methane and ethylene in electrochemical reduction of carbon dioxide at copper electrode in aqueous hydrogen carbonate solution, *Chem. Lett.* 1986, **15**, 897.
11. M. Halmann, Photoelectrochemical reduction of aqueous carbon dioxide on p-type gallium phosphide in liquid junction solar cells, *Nature* 1978, **275**, 115.
12. E. Gileadi, Electrode Kinetics for Chemists, Engineers, and Materials Scientists, Wiley VCH, Weinheim, Germany 1993.
13. Y. Garsany, O. A. Baturina, K.E. Swider Lyons, S.S. Kocha, Experimental Methods for Quantifying the Activity of Platinum Electrocatalysts for the Oxygen Reduction Reaction, *Anal. Chem*. 2010, **82**, 632.
14. X. Li, J. Wen, J. Low, Y. Fang, J. Yu, Design and fabrication of semiconductor photocatalyst for photocatalytic reduction of CO_2 to solar fuel, *Sci. China Mater*. 2014, **57**, 70.
15. X. Chen, S.S. Mao, Titanium Dioxide Nanomaterials: Synthesis, Properties, Modifications, and Applications, *Chem. Rev*. 2007, **107**, 2891.
16. J. Low, B. Cheng, J. Yu, Surface modification and enhanced photocatalytic CO_2 reduction performance of TiO_2: a review, *Appl. Surf. Sci*. 2017, **392**, 658.
17. Q. Huang, J. Yu, S. Cao, C. Cui, B. Cheng, Efficient photocatalytic reduction of CO_2 by amine-functionalized g-C_3N_4, *Appl. Surf. Sci*. 2015, **358**, 350.
18. J.R. Bolton, S.J. Strickler, J.S. Connolly, Limiting and realizable efficiencies of solar photolysis of

water, *Nature* 1985, **316**, 495.

19. C.R. Cox, J.Z. Lee, D.G. Nocera, T. Buonassisi, Ten-percent solar-to-fuel conversion with nonprecious materials, *Proc. Natl. Acad. Sci. USA* 2014, **111**, 14057.
20. M. Tahir, N.S. Amin, Advances in visible light responsive titanium oxide-based photocatalysts for CO_2 conversion to hydrocarbon fuels, *Energy Convers. Manag*., **76** (2013), pp. 194-214.
21. Y. Xia, J.Y. Reaction, rational design of highly active photocatalysts for CO_2 conversion, *Chem*, **6** (2020), pp. 1039-1040.
22. X.D. Wang, Y.H. Huang, J.F. Liao, Y. Jiang, L. Zhou, X.Y. Zhang, *et al.,* In situ construction of a Cs_2SnI_6 perovskite nanocrystal/SnS_2 nanosheet heterojunction with boosted Interfacial charge transfer, *J. Am. Chem. Soc*., **141** (2019), pp. 13434-13441.
23. P. Zhou, X. Wang, S. Yan, Z. Zou, Solid solution photocatalyst with spontaneous polarization exhibiting low recombination toward efficient CO_2 photoreduction, *ChemSusChem*, **9** (2016), pp. 2064-2068.
24. F. Chu, S. Li, H. Chen, L. Yang, O. Ola, M. Maroto-Valer, *et al.,* Modeling photocatalytic conversion of carbon dioxide in bubbling twin reactor, *Energy Convers. Manage*., **149** (2017), pp. 514-525.
25. K. Yuan, L. Yang, X. Du, Y. Yang, Performance analysis of photocatalytic CO_2 reduction in optical fiber monolith reactor with multiple inverse lights, *Energy Convers. Manag*., **81** (2014), pp. 98-105.
26. X. Huang, Q. Shen, J. Liu, N. Yang, G. Zhao, A CO_2 adsorption-enhanced semiconductor / metal-complex hybrid photoelectrocatalytic interface for efficient formate production, *Energy Environ Sci*, **9** (2016), pp. 3161-3171.
27. S. Feng, X. Chen, Y. Zhou, W. Tu, P. Li, H. Li, *et al.,* $Na_2V_6O_{16}\cdot xH_2O$ nanoribbons: large-scale synthesis and visible-light photocatalytic activity of CO_2 into solar fuels, *Nanoscale*, **6** (2014), pp. 1896-1900.
28. B. Qin, Y. Li, H. Wang, G. Yang, Y. Cao, H. Yu, *et al.,* Efficient electrochemical reduction of CO_2 into CO promoted by sulfur vacancies, *Nano Energy*, **60** (2019), pp. 43-51.
29. H. Wang, L. Zhang, K. Wang, X. Sun, W. Wang, Enhanced photocatalytic CO_2 reduction to methane over $WO_3\cdot 0.33H_2O$ via Mo doping, *Appl. Catal. B*, **243** (2019), pp. 771-779.
30. J. Albo, M. Alvarez-Guerra, P. Castaño, A. Irabien, Towards the electrochemical conversion of carbon dioxide into methanol, *Green Chem*., **17** (2015), pp. 2304-2324.
31. M. Subrahmanyam, S. Kaneco, N. Alonso-Vante, A screening for the photo reduction of carbon dioxide supported on metal oxide catalysts for C_1–C_3 selectivity, *Appl. Catal. B*, **23** (1999), pp. 169-174.
32. N. Sasirekha, S.J.S. Basha, K. Shanthi, Photocatalytic performance of Ru doped anatase mounted on silica for reduction of carbon dioxide, *Appl. Catal. B*, **62** (2006), pp. 169-180
33. E. Karamian, S. Sharifnia, On the general mechanism of photocatalytic reduction of CO_2, *J. CO_2. Util*., **16** (2016), pp. 194-203.
34. J.Y. Liu, X.Q. Gong, A.N. Alexandria, Mechanism of CO_2 photocatalytic reduction to methane and methanol on defected anatase TiO_2 (101): a density functional theory study, *J. Phys. Chem. C*, **123** (2019), pp. 3505-3511.
35. F.L. Li, H.J. Zhang, Synthesis of hollow sphere and 1D structural materials by sol-gel process, *Materials*, **10** (2017).
36. X.Y. Yang, L.H. Chen, Y. Li, J.C. Rooke, C. Sanchez, B.-L. Su, Hierarchically porous materials: synthesis strategies and structure design, *Chem. Soc. Rev*., **46** (2017), pp. 481-558.
37. Y. Li, J. Shi, Hollow-structured mesoporous materials: chemical synthesis, functionalization and applications, *Adv. Mater*., **26** (2014), pp. 3176-3205.
38. J. Sun, G. Chen, J. Wu, H. Dong, G. Xiong, Bismuth vanadate hollow spheres: Bubble template synthesis and enhanced photocatalytic properties for photodegradation, *Appl. Catal. B: Environ*., **132** (2013), pp. 304-314.
39. Y. Li, J. Liu, X. Huang, G. Li, Hydrothermal synthesis of Bi_2WO_6 uniform hierarchical microspheres, *Cryst. Growth Des*., **7** (2007), pp. 1350-1355.

40. R. Buonsanti, V. Grillo, E. Carlino, C. Giannini, T. Kipp, R. Cingolani, P.D. Cozzoli, Nonhydrolytic synthesis of high-quality anisotropically shaped brookite TiO_2 nanocrystals, *J. Am. Chem. Soc*., **130** (2008), pp. 11223-11233.
41. J. Yu, C.Y. Xu, F.X. Ma, S.P. Hu, Y.W. Zhang, L. Zhen, Monodisperse SnS_2 nanosheets for high-performance photocatalytic hydrogen generation, *ACS Appl. Mater. Interfaces*, **6** (2014), pp. 22370-22377.
42. H. Yang, X.L. Wu, M.H. Cao, Y.G. Guo, Solvothermal synthesis of $LiFePO_4$ hierarchically dumbbell-like microstructures by nanoplate self-assembly and their application as a cathode material in lithium-ion batteries, *J.* Phys. Chem. C, **113** (2009), pp. 3345-3351.
43. X.-K. Wang, C. Wang, W.-Q. Jiang, W.-L. Guo, J.-G. Wang, Sonochemical synthesis and characterization of Cl-doped TiO_2 and its application in the photodegradation of phthalate ester under visible light irradiation, *Chem. Eng. J*., **189** (2012), pp. 288-294.
44. J. Fu, G.Z. Kyzas, Z. Cai, E.A. Deliyanni, W. Liu, D. Zhao, Photocatalytic degradation of phenanthrene by graphite oxide-TiO_2-$Sr(OH)_2$/$SrCO_3$ nanocomposite under solar irradiation: effects of water quality parameters and predictive modeling, *Chem. Eng. J*., **335** (2018), pp. 290-300.
45. J. Jiang, Q. Zhang, X. Zhan, F. Chen, A multifunctional gelatin-based aerogel with superior pollutants adsorption, oil/water separation and photocatalytic properties, *Chem. Eng. J*., **358** (2019), pp. 1539-1551.
46. M. Li, C. Bian, G. Yang, X. Qiang, Facile fabrication of water-based and non-fluorinated superhydrophobic sponge for efficient separation of immiscible oil/water mixture and water-in-oil emulsion, *Chem. Eng. J*., **368** (2019), pp. 350-358.
47. T. Razpotnik, J. Macek, Synthesis of nickel oxide/zirconia powders via a modified Pechini method, *J. Eur. Ceram. Soc*. **27** (2007) 1405–1410.
48. M.P. Pechini, Method of Preparing Lead and Alkaline-Earth Titanates and Niobates and Coating Method Using the Same to Form a Capacitor-US PAT., **3.**330.697, 1967.
49. X. Chen, S. Shen, L. Guo, S. S. Mao, Semiconductor-based Photocatalytic Hydrogen Generation, *Chem. Rev*. 2010, **110**, 6503.
50. Y. Sohn, W. Huang, F. Taghipour, Recent progress and perspectives in the photocatalytic CO_2 reduction of Ti-oxide-based nanomaterials, *Appl. Surf. Sci*. 2017, **396**, 1696.
51. J. Pan, G. Liu, G. Q. M. Lu, H. M. Cheng, On the True Photo reactivity Order of {001}, {010}, and {101} Facets of Anatase TiO_2 Crystals, *Angew. Chem., Int. Ed*. 2011, **50**, 2133.
52. B.R. Eggins, J.T. Irvine, E.P. Murphy, J. Grimshaw, Formation of two-carbon acids from carbon dioxide by photoreduction on cadmium sulphide, *J. Chem. Soc. Chem. Commun*. 1988, **16**, 1123.
53. B. AlOtaibi, X. Kong, S. Vanka, S. Y. Woo, A. Pofelski, F. Oudjedi, S. Fan, M. G. Kibria, G. A. Botton, W. Ji, H. Guo, Z. Mi, Photochemical Carbon Dioxide Reduction on Mg-Doped Ga(In)N Nanowire Arrays under Visible Light Irradiation, *ACS Energy Lett*. 2016, **1**, 246.
54. Y. Izumi, Recent advances in the photocatalytic conversion of carbon dioxide to fuels with water and/or hydrogen using solar energy and beyond, *Coord. Chem. Rev*. 2013, **257**, 171.
55. X.L. Luo, Z. Yin, M.H. Zeng, M. Kurmoo, The construction, structures, and functions of pillared layer metal–organic frameworks, *Inorg. Chem. Front*. 2016, **3**, 1208.
56. Y. Hori, K. Kikuchi, A. Murata, S. Suzuki, Production of methane and ethylene in electrochemical reduction of carbon dioxide at copper electrode in aqueous hydrogen carbonate solution, *Chem. Lett*. 1986, **15**, 897.
57. Y. Hori, A. Murata, R. Takahashi, Formation of hydrocarbons in the electrochemical reduction of carbon dioxide at a copper electrode in aqueous solution, *J. Chem. Soc., Faraday Trans. 1* 1989, **85**, 2309.
58. Y. Hori, H. Wakebe, T. Tsukamoto, O. Koga, Electrocatalytic process of CO selectivity in electrochemical reduction of CO_2 at metal electrodes in aqueous media, *Electrochim. Acta* 1994, **39**, 1833.
59. X. Hong, K. Chan, C. Tsai, J. K. Nørskov, How Doped MoS_2 Breaks Transition-Metal Scaling Relations

for CO_2 Electrochemical Reduction, *ACS Catal*. 2016, **6**, 4428.

60. S. Zhang, P. Kang, S. Ubnoske, M. K. Brennaman, N. Song, R. L. House, J. T. Glass, T. J. Meyer, Polyethyleneimine-Enhanced Electrocatalytic Reduction of CO_2 to Formate at Nitrogen-Doped Carbon Nanomaterials, *J. Am. Chem. Soc*. 2014, **136**, 7845.
61. J. Wu, R. M. Yadav, M. Liu, P. P. Sharma, C. S. Tiwary, L. Ma, X. Zou, X. D. Zhou, B. I. Yakobson, J. Lou, P. M. Ajayan, Achieving Highly Efficient, Selective, and Stable CO_2 Reduction on Nitrogen-Doped Carbon Nanotubes, *ACS Nano* 2015, **9**, 5364.
62. O, Zambaga., Y.C, Kwang., W.C, Oh. Novel Micro and Nanostructure of $AgCuInS_2$-Graphene-TiO_2 Ternary Composite for Photocatalytic CO_2 Reduction for Methanol, *Fuel*, 5 (2020), 26389–26401.
63. Y, Ya-hui., X, Ren-rui, L, Hang., L, Can-jun., L, Wen-hua., Z, Fa-qi. Photoelectrocatalytic reduction of CO_2 into formic acid using WO_{3-x} /TiO_2 film as novel photoanode, *T. Nonferr. Metal. Soc.,* 2016, 26 (9), 2390-2396.
64. A.A Ensafi., H.A, Alinajafi., B, Rezaei. Pt-modified nitrogen doped reduced graphene oxide: a powerful electrocatalyst for direct CO_2 reduction to methanol. *J Electroanal. Chem,* 2016, 783, 82-89.
65. R. Reske, H. Mistry, F. Behafarid, B. Roldan Cuenya, P. Strasser, Particle Size Effects in the Catalytic Electroreduction of CO_2 on Cu Nanoparticles, *J. Am. Chem. Soc*. 2014, **136**, 6978.
66. K. Manthiram, B. J. Beberwyck, A. P. Alivisatos, Enhanced Electrochemical Methanation of Carbon Dioxide with a Dispersible Nanoscale Copper Catalyst, *J. Am. Chem. Soc*. 2014, **136**, 13319.
67. W. Zhu, R. Michalsky, O. Metin, H. Lv, S. Guo, C. J. Wright, X. Sun, A. A. Peterson, S. Sun, Monodisperse Au Nanoparticles for Selective Electrocatalytic Reduction of CO_2 to CO, *J. Am. Chem. Soc*. 2013, **135**, 16833.
68. S. Back, M. S. Yeom, Y. Jung, Active Sites of Au and Ag Nanoparticle Catalysts for CO_2 Electroreduction to CO, *ACS Catal*. 2015, **5**, 5089.
69. A. Salehi Khojin, H. R. M. Jhong, B. A. Rosen, W. Zhu, S. Ma, P. J. A. Kenis, R. I. Masel, Nanoparticle Silver Catalysts That Show Enhanced Activity for Carbon Dioxide Electrolysis, *J. Phys. Chem. C* 2013, **117**, 1627.
70. M. Zeng, Y. Li, Recent advances in heterogeneous electrocatalysts for the hydrogen evolution reaction, *J. Mater. Chem. A* 2015, **3**, 14942.
71. M. Asadi, B. Kumar, A. Behranginia, B. A. Rosen, A. Baskin, N. Repnin, D. Pisasale, P. Phillips, W. Zhu, R. Haasch, R. F. Klie, P. Kral, J. Abiade, A. Salehi Khojin, Robust carbon dioxide reduction on molybdenum di-sulphide edges, *Nat. Commun*. 2014, **5**, 4470.
72. G. Xi, S. Ouyang, P. Li, J. Ye, Q. Ma, N. Su, H. Bai, C. Wang, Ultrathin $W_{18}O_{49}$ Nanowires with Diameters below 1 nm: Synthesis, Near Infrared Absorption, Photoluminescence, and Photochemical Reduction of Carbon Dioxide, *Angew. Chem., Int. Ed*. 2012, **51**, 2395.
73. T. Wang, X. Meng, G. Liu, K. Chang, P. Li, Q. Kang, L. Liu, M. Li, S. Ouyang, J. Ye, *In situ* synthesis of ordered mesoporous Co-doped TiO_2 and its enhanced photocatalytic activity and selectivity for the reduction of CO_2, *J. Mater. Chem. A* 2015, **3**, 9491.
74. V. P. Indrakanti, J. D. Kubicki, H. H. Schobert, Photoinduced activation of CO_2 on Ti-based heterogeneous catalysts: Current state, chemical physics-based insights and outlook, *Energy Environ. Sci*. 2009, **2**, 745.
75. Z. Zhang, Y. Huang, K. Liu, L. Guo, Q. Yuan, B. Dong, Multichannel-Improved Charge Carrier Dynamics in Well-Designed Hetero-nanostructural Plasmonic Photocatalysts toward Highly Efficient Solar to Fuels Conversion, *Adv. Mater.* 2015, **27**, 5906.
76. [a]. Neaþu, J. A. Maciá Agulló, P. Concepción, H. Garcia, Gold–Copper Nanoalloys Supported on TiO_2 as Photocatalysts for CO_2 Reduction by Water, *J. Am. Chem. Soc*. 2014, **136**, 15969.
77. W.N. Wang, W.J. An, B. Ramalingam, S. Mukherjee, D.M. Niedzwiedzki, S. Gangopadhyay, P. Biswas, Size and Structure Matter: Enhanced CO_2 Photoreduction Efficiency by Size-Resolved Ultrafine Pt Nanoparticles on TiO_2 Single Crystals., *J. Am. Chem. Soc*. 2012, **134**, 11276.